Chemical Engineering Journal 261 (2015) 67–75

Contents lists available at ScienceDirect

Chemical Engineering Journal

journal homepage: www.elsevier.com/locate/cej

Modeling of photocatalytic degradation of organic components in water by nanoparticle suspension

Hagen Eckert [a,b,*], Manfred Bobeth [a,b], Sara Teixeira [a], Klaus Kühn [a], Gianaurelio Cuniberti [a,b,c]

[a] Institute for Materials Science and Max Bergmann Center of Biomaterials, TU Dresden, 01062 Dresden, Germany
[b] Dresden Center for Computational Materials Science (DCCMS), TU Dresden, 01062 Dresden, Germany
[c] Center for Advancing Electronics Dresden, TU Dresden, 01062 Dresden, Germany

HIGHLIGHTS

- Development of a model for the kinetic processes in photocatalytic water purification.
- Experiments with ciprofloxacin and methylene blue in TiO_2 and ZnO nanosuspensions.
- Estimation of model parameters from comparison with experimental findings.
- Calculated concentration evolution of degradation intermediates.
- Simulated TOC curves for different model assumptions.

ARTICLE INFO

Article history:
Available online 27 June 2014

Keywords:
Photocatalysis
Modeling
TiO_2
ZnO
Ciprofloxacin
Methylene blue

ABSTRACT

Photocatalytic degradation of organic components in water by means of TiO_2 nanosuspensions under ultraviolet (UV) irradiation represents an efficient method for water purification. In the present paper, a modeling approach is proposed to simulate the involved kinetic processes based on the Langmuir–Hinshelwood mechanism. The extended model also includes the formation of intermediate organic components either by an incremental degradation mechanism or by a fragmentation mechanism. Model parameters were estimated from comparison with experimental findings. To demonstrate these models, adsorption and degradation experiments were performed using the antibiotic ciprofloxacin and the dye methylene blue as organic compounds and TiO_2 and ZnO as photocatalytic materials. By comparing our simulations with concentration measurements, we found that the adsorption of organic molecules on the surface of the photocatalyst was rate determining at an irradiation intensity of about 20 W m^{-2}. The derived adsorption rates for ZnO were considerably higher than those for TiO_2. The calculated concentration evolution of intermediates as well as the TOC evolution are discussed for different model assumptions with respect to their desorption rates from the photocatalyst surface.

1. Introduction

Many pollutants, such as heavy metals, dyes, and pharmaceuticals are discharged into the water cycle at many stages in our daily lives. In particular, antibiotics represent a serious problem because of their toxicity to microflora and -fauna, and of the possible development of antibiotic-resistant microorganisms [1–3]. Global over- and abuse of antibiotics has resulted in their concentrations steadily increasing in wastewater [4]. Another common pollutants are dyes, which are widely used in various industries and which are often released into the wastewater. Some dyes are toxic, mutagenic [5] or carcinogenic [6] and should therefore be removed from wastewater.

Photocatalytic oxidation is a promising approach in the purification of water, which is contaminated with organic pollutants [7–11]. Successful degradation experiments have been reported [7] for various organic molecules, such as azo dyes [12], furfural [13], sulfamethoxazole [14], and acetylene [15]. An efficient way to study the photocatalytic oxidation process is the application of suspensions of photocatalytic nanoparticles, since these suspensions exhibit a large specific surface area. For example, the anatase phase of TiO_2 is known for its good photocatalytic properties [16,17].

* Corresponding author at: Institute for Materials Science, TU Dresden, 01062 Dresden, Germany. Tel.: +49 351 463 31461.
E-mail address: hagen.eckert@tu-dresden.de (H. Eckert).

http://dx.doi.org/10.1016/j.cej.2014.05.147
1385-8947/

Nomenclature

a	particle spacing (m)
A(ad)	adsorbed organic molecule
A(aq)	organic molecule in solution
a_s	specific surface area (m^{-1})
A_m	surface area covered per molecule (m^2)
$C_{A(ad)}$	concentration of adsorbed organic molecules (m^{-2})
$C_{A(aq)}$	concentration of organic molecules in solution (m^{-3})
$C_{A(aq),0}$	initial concentration of organic molecules in solution (m^{-3})
$C_{A(aq),\infty}$	equilibrium concentration of organic molecules in solution (m^{-3})
$C_{M(aq)}$	concentration of mineralized components in solution (m^{-3})
C_P	particle concentration (m^{-3})
D	diffusion coefficient ($m^2\ s^{-1}$)
$E_{0/1}$	fit parameters for k_{des}
E_{des}	desorption energy (J)
I_0	photon flux ($m^{-2}\ s^{-1}$)
j_{ads}	adsorption flux ($m^{-2}\ s^{-1}$)
j_{des}	desorption flux ($m^{-2}\ s^{-1}$)
j_{reac}	reaction flux ($m^{-2}\ s^{-1}$)
k_{ads}	adsorption rate constant ($m\ s^{-1}$)
k_{app}	apparent rate constant (s^{-1})
k_B	Boltzmann constant ($J\ K^{-1}$)
k_{des}	desorption rate constant (s^{-1})
k_{reac}	reaction rate constant (s^{-1})
M	mineralized components
n	molecule size index
T	temperature (K)
t	time (s)
t_D	characteristic diffusion time (s)
$\alpha_{0/1}$	parameters for v_0
$\beta_{0/1}$	parameters for E_{des}
η	viscosity
κ	adsorption prefactor (m)
v_0	pre-exponential factor (s^{-1})
ϕ	quantum yield
Θ	surface coverage

The simulation of the kinetic processes, which are involved in the photocatalytic oxidation of organic pollutants, are expected to lead to a deeper quantitative understanding of the whole mineralization process. This could also help in optimizing the design of reactors for photocatalytic water purification. A very important issue of reactor design is the radiation transport in the reaction volume, investigated for example in [18–20]. The degradation kinetics of organic pollutants has often been described within the framework of the Langmuir–Hinshelwood (LH) model (see e.g. [10] and references therein). For example, Minero [21] discussed several kinetic models of the photocatalytic process with the aim to obtain equations with physical meaning and reduced complexity. An experimental validation of reported kinetic models has been performed by Andreozzi et al. [22] for the photocatalytic degradation of 4-nitrophenol. The LH model combined with a Lambert–Beer type model for the radiation transport has been applied to describe the degradation of methylene blue by Sannino et al. [23].

Generally, the photocatalytic mineralization of organic molecules is a complex process, where parts of the initial molecules are oxidized step by step on the catalyst surface in the presence of photo-generated radicals. These radicals may also destroy the molecules' bonds thereby breaking them into smaller molecules. These molecules may then desorb from the surface of the photocatalyst. Consequently, various intermediate molecules of different sizes emerge in the solution. In the present study, we propose two model approaches of photocatalytic degradation which extend models with only one molecule species [10,23,24] by including the evolution of intermediates. In a first limiting case, we study degradation by successive oxidation of the elements of the initial molecules, excluding the possibility of molecule fragmentation. Within a second complementary model, random fragmentation of organic molecules into smaller intermediates and oxidation of the smallest fragments is considered. Investigations of the concentration evolution of intermediates have been presented for example in [25–27]. A comprehensive experimental analysis and theoretical modeling of the degradation of phenol has been reported in [26,27]. The kinetic model was based on a 'series–parallel' reaction network which included several intermediate species. The model parameters were fitted from measured concentration profiles of intermediates in the solution. In the present paper, we propose a model approach where, besides the concentrations in the solution, we explicitly include also the dynamics of the surface concentrations of adsorbed intermediates. In particular, we demonstrate the effect of different desorption properties of intermediates on their concentration evolution.

Our theoretical analysis was compared with degradation experiments performed on the antibiotic ciprofloxacin [28–30] and on the dye methylene blue [23,24,31] in a photocatalytic slurry. Nanoparticles of TiO_2 and ZnO were used as photocatalysts. This way, we attempted to obtain characteristic values for kinetic model parameters. Additionally, we compared also with literature data on the degradation of methylene blue [31].

This paper is organized as follows. After a brief presentation of the experimental investigations, different mathematical models to describe the degradation process of the organic compounds in the solution are presented. Thereafter, our degradation experiments are presented and rate constants in our model are determined by fitting to these measurements. Finally, simulations of the concentration evolution of the initial and intermediate organic molecules, and of the total organic carbon (TOC) in the solution, are discussed.

2. Materials and methods

2.1. Experimental investigations

For performing adsorption experiments in the dark and degradation experiments under UVA, aqueous solutions of 12.5 μM ciprofloxacin and 11.0 μM methylene blue were prepared. To those solutions, 1 g L^{-1} of TiO_2 P25 (Evonik) or ZnO (IOLITEC Ionic Liquids Technologies GmbH) was added under constant stirring. The textural properties of the photocatalyst nanoparticles were analyzed at 77 K by nitrogen adsorption–desorption in a Micromeritics TriStar analyzer (Micromeritics, Norcross GA). Before performing adsorption experiments, samples (0.5 g) were outgassed at 26.7 Pa and 350 °C for 6 h. The specific surface area of the particles was determined by the Brunauer–Emmett–Teller (BET) method.

In all experiments, the samples were analyzed using a Varian CARY-100 UV–VIS spectrophotometer. The concentrations were calculated by comparing the measured absorption spectra to the calibration curves.

For the absorption experiments in the dark, a sample was taken using a syringe and then pressed through a filter (Rotilabo nylon,

pore size 0.2 μm) 40 s after the photocatalytic nanoparticles were added. This procedure was then repeated several times. All samples were centrifuged for 60 min, after which the supernatant was removed. After the sample was centrifuged for another 60 min, the concentration of the organic compound in the new supernatant was measured.

The degradation experiments were carried out in 100 ml borosilicate-glass beakers from VWR with 3.3 mm wall thickness and 5 cm diameter. Prior to the degradation experiments, samples were stirred in the dark for 30 min so that an adsorption–desorption equilibrium of the organic molecules on the photocatalyst surface was obtained. An amount of 50 ml of this solution was then exposed under continuous stirring to UVA-radiation with an intensity peak at 365 nm. The illuminating device was equipped with 6 Philips 8 W mercurial fluorescent tubes manufactured by UMEX. Two beakers were placed in 15 cm distance from the illumination device. The UV intensity ranged from 18 to 19 W m^{-2} and was determined by a UV34 Lux Meter (PCE). For analyzing the temporal degradation of organic molecules, samples were taken from the solution at certain time intervals and subsequently filtered and centrifuged to remove the catalyst nanoparticles.

2.2. Modeling approach

The processes, occurring during photocatalytic degradation of organic components in the solution, are illustrated in Fig. 1. We consider here the case where mineralization of organic molecules takes place mainly at the surface of the photocatalytic material. Possible reactions of radicals and organic compounds in the water are neglected. The organic components diffuse to the surface of the photocatalytic nanoparticles, where they are adsorbed and mineralized. In competition to the process of mineralization is the desorption and diffusion of the organic molecules away from the photocatalytic particles. In our modeling approach, we suppose that the oxygen supply for mineralization is sufficient during the entire process.

At the beginning of this complex process, starting from a homogeneous concentration of organic molecules, their adsorption at the nanoparticle surface could lead to a slight concentration gradient around the particles, depending on the adsorption rate. However, the concentration profile strongly flattens in a very short time due to the relatively fast diffusion of the organic molecules in the solution. By means of the Stokes–Einstein equation

$$D = k_B T/(6\pi\eta r) \tag{1}$$

where $\eta = 10^{-3}$ Pa s is the dynamic viscosity of water and $r = 0.4$ nm is the radius of a sphere with volume equal to the van-der-Waals volume of ciprofloxacin, we find a diffusion coefficient of 5.2×10^{-10} m^2 s^{-1}. A similar value of 6.7×10^{-10} m^2 s^{-1} is obtained when using the empirical equation presented by Wilke and Chang [32]. The order of magnitude of the diffusion distance to the nanoparticles, which the molecules have to cover, is given by $a = C_P^{-1/3}$, where C_P is the particle concentration. For a particle suspension of 1 g L^{-1} TiO_2 and an upper estimate of the particle radius of 50 nm (considering possible agglomeration), one finds for example $a \approx 1300$ nm and a characteristic diffusion time $t_D = a^2/D = 2.5 \times 10^{-3}$ s [33]. Since this time is orders of magnitude smaller than the time, where significant mineralization of the organic molecules occurs, an almost homogeneous molecule concentration between nanoparticles can be assumed in the following approaches.

2.2.1. Single organic species model

In our modeling approach, we follow at first previous studies (see for example [10,12] and references therein) and consider an idealized model system with only one organic species in aqueous solution. The organic molecules in the solution adsorb onto the particle and are mineralized due to photocatalytic reactions as expressed by the reaction equations

$$A(aq) \leftrightarrows A(ad) \rightarrow M(aq) \tag{2}$$

The molecules can also desorb before mineralization. This applies especially to experiments performed in the dark, where mineralization does not occur. Temporal changes of the molecule concentration in the solution $C_{A(aq)}$ (in m^{-3}) and the concentration on the photocatalyst particle surface $C_{A(ad)}$ (in m^{-2}) are given by

$$\frac{d}{dt}C_{A(ad)} = j_{ads} - j_{des} - j_{reac} \tag{3}$$

$$\frac{d}{dt}C_{A(aq)} = a_s(j_{des} - j_{ads}) \tag{4}$$

These equations include the specific surface area of the nanoparticles a_s and different molecule fluxes

$$j_{ads} = k_{ads}(1 - \Theta)C_{A(aq)} \tag{5}$$

$$j_{des} = k_{des}C_{A(ad)} \tag{6}$$

$$j_{reac} = k_{reac}C_{A(ad)} \tag{7}$$

The adsorption flux j_{ads} is proportional to the molecule concentration in the solution and the free surface area of the particles, assuming that only one monolayer is formed. The surface coverage Θ is given by $\Theta = A_m C_{A(ad)}$ with A_m as the surface area covered by one molecule. This area was estimated by the largest possible projection of the Connolly surface [34] around the three-dimensional molecule structure (probe molecule: water, $r = 1.4$ Å), which was calculated by using the software pymol [35]. The reaction flux j_{reac} describes the number of mineralized molecules per area and time. Both desorption and reaction fluxes are proportional to the concentration of organic molecules on the surface. In the limiting case of small surface coverage $\Theta \ll 1$, the system of ordinary differential equations, Eqs. (3) and (4), becomes linear and can be solved analytically (cf. Appendix).

The rate constants k_{ads}, k_{des}, and k_{reac} can be derived from the experimentally obtained data. First the adsorption and desorption rates are obtained from experiments of the concentration

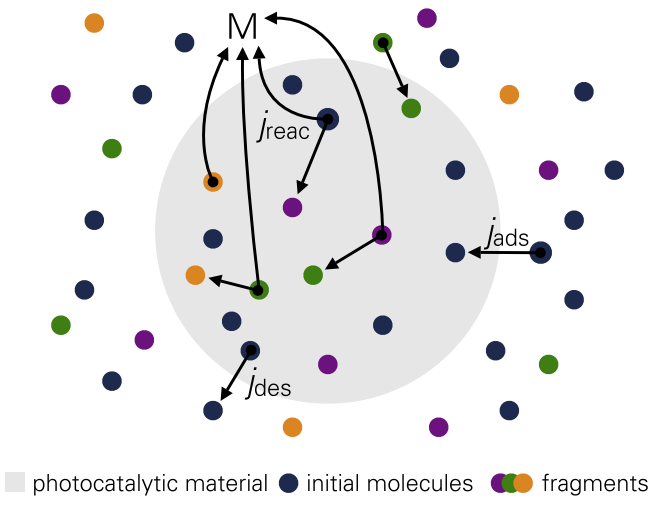

Fig. 1. Illustration of processes occurring during mineralization of organic molecules at the surface of photocatalytic nanoparticles in solution. Due to degradation and desorption, various intermediate organic molecules (fragments) can emerge on the surface and in the solution.

evolution $C_{A(aq)}(t)$ in the dark. After an initial decrease of the concentration, a stationary value is reached due to adsorption–desorption equilibrium at the particle surface. For sufficiently dilute molecule concentration, the emerging coverage on the particle surface is very small: $\Theta \ll 1$. Then, the concentration evolution results as solution of Eq. (3) with $j_{reac} = 0$

$$C_{A(aq)}(t) = C_{A(aq),0} \frac{\exp[-(k_{ads}a_s + k_{des})t] + k_{des}(k_{ads}a_s)^{-1}}{1 + k_{des}(k_{ads}a_s)^{-1}} \tag{8}$$

Generally, the adsorption rate constants can be determined from accurate measurements of the initial concentration change $dC_{A(aq)}/dt$ at $t = 0$, when the coverage is still negligible

$$k_{ads} = -\frac{\dot{C}_{A(aq)}(0)}{a_s C_{A(aq),0}} \tag{9}$$

With the knowledge of k_{ads}, the desorption rate constant k_{des} is then obtained from the measured asymptotic concentration value $C_{A(aq),\infty} = C_{A(aq)}(t \to \infty)$. From the adsorption–desorption equilibrium $j_{ads} = j_{des}$, we find with $\Theta = A_m C_{A(ad)}$

$$k_{des} = k_{ads}(1 - A_m C_{A(ad),\infty}) \frac{C_{A(aq),\infty}}{C_{A(ad),\infty}} \tag{10}$$

where the asymptotic surface concentration follows from the total particle balance as

$$C_{A(ad),\infty} = a_s^{-1}(C_{A(aq),0} - C_{A(aq),\infty}). \tag{11}$$

After determination of the rate constants k_{ads} and k_{des} by means of experiments conducted in the dark, the reaction rate constant k_{reac} is determined from concentration measurements obtained in the degradation experiments under illumination. In this fitting procedure, Eqs. (3) and (4) are solved numerically.

For the case of a fast establishment of an adsorption–desorption equilibrium with quasi-stationary surface concentration $\dot{C}_{A(ad)} = 0$ (i.e. $|\dot{C}_{A(ad)}| \ll k_{ads}C_{A(aq)},\ k_{des}C_{A(ad)}$), the surface concentration in the system of Eqs. (3) and (4) can be eliminated. The solution of Eq. (3) in the limit of small coverage $\Theta \ll 1$ reads then $C_{A(ad)} = C_{A(aq)}k_{ads}(k_{des} + k_{reac})^{-1}$. Insertion of this expression into Eq. (4) yields $\dot{C}_{A(aq)} = -k_{app}C_{A(aq)}$ with the solution

$$C_{A(aq)}(t) = C_{A(aq),0} \exp(-k_{app}t) \tag{12}$$

where the apparent degradation rate constant is given by

$$k_{app} = a_s k_{ads} k_{reac}(k_{des} + k_{reac})^{-1} \tag{13}$$

Thus, for $k_{des} \ll k_{reac}$, we find $k_{app} = a_s k_{ads}$. This means that the degradation rate becomes adsorption-limited and does not depend on the reaction rate constant. In the opposite case, $k_{des} \gg k_{reac}$, one obtains $k_{app} = a_s k_{ads} k_{reac}/k_{des}$. Then, the degradation rate is proportional to the reaction rate constant.

2.2.2. Multiple organic species model

The single organic species model is appropriate for analyzing the adsorption–desorption process of the initial organic compounds. However, photocatalytic mineralization of organic molecules is a complex process, accompanied by the formation of various intermediates in several reaction steps. Therefore, we consider two idealized mechanisms of the mineralization reaction (Fig. 2). In the first model, the initial organic molecule is oxidized step by step, i.e. only a small part (e.g. one carbon atom) is oxidized in one step (Fig. 2a). This model is thus referred to as incremental oxidation model. In the second model, referred to as fragmentation model, we consider the possibility that bonds within the molecule are destroyed due to photocatalytic reactions so that the molecule breaks into smaller molecules (Fig. 2b). In both models, also intermediates may desorb from the catalyst surface. Thus, we have to introduce concentrations of different species in the solution and on the surface of the catalyst. The different species will be characterized solely by their size.

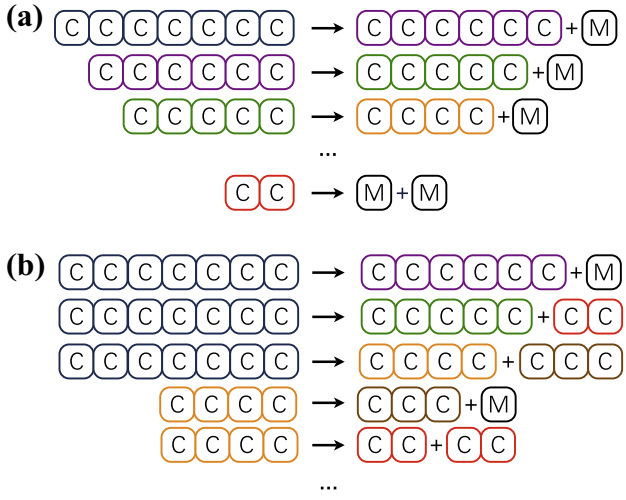

Fig. 2. Illustration of reaction steps in the two multiple organic species models: (a) incremental oxidation and removal of single carbon atoms and (b) formation of fragments of molecules by bond breaking and subsequent oxidation of the smallest fragments.

2.2.2.1. Incremental oxidation model. As an example, we consider here initial organic compounds and their intermediates, which are distinguished by their number of carbon atoms n. Within the incremental oxidation model, the molecule degradation is described in an idealized manner by oxidation and removal of one carbon atom in every reaction step (Fig. 2a). Adsorption, desorption, and mineralization of a molecule of size n can therefore be expressed by the reaction equations

$$A_n(aq) \leftrightarrows A_n(ad) \rightarrow A_{(n-1)}(ad) + M(aq) \tag{14}$$

The concentration evolution of molecules of size $n \geqslant 2$ and of the mineralized component are given by

$$\frac{d}{dt}C_{A_n(ad)} = j_{n,ads} - j_{n,des} - j_{n,reac} + j_{(n+1),reac} \tag{15}$$

$$\frac{d}{dt}C_{A_n(aq)} = a_s(j_{n,des} - j_{n,ads}) \tag{16}$$

$$\frac{d}{dt}C_{M(aq)} = a_s\left(2j_{2,reac} + \sum_{n=3}^{n_{max}} j_{n,reac}\right) \tag{17}$$

with the fluxes given by

$$j_{n,ads} = k_{n,ads}(1 - \Theta)C_{A_n(aq)} \tag{18}$$

$$j_{n,des} = k_{n,des}C_{A_n(ad)} \tag{19}$$

$$j_{n,reac} = k_{n,reac}C_{A_n(ad)} \tag{20}$$

The flux $j_{(n+1),reac}$ in Eq. (15) describes the formation of molecules of size n due to oxidation of molecules of size $n + 1$. To track the evolution of the concentration of the mineralized component C_M in the solution, the reaction fluxes due to mineralization of all molecules are summed in Eq. (17). For simplicity, we assume the rate constants in Eqs. (21)–(23) to vary only with the molecule size n

$$k_{n,\mathrm{ads}} = \kappa D_n \tag{21}$$

$$k_{n,\mathrm{des}} = \nu_0(n)\exp\left(-\frac{E_{\mathrm{des}}(n)}{k_B T}\right) \tag{22}$$

$$k_{n,\mathrm{reac}} = I_0\,\phi A_n \tag{23}$$

This simplifying assumption has been made since the size of molecules should considerably affect the rate constants. Which seems particularly appropriate for chain molecules with equal repeating units. In general, the rate constants depend of course also on the specific element composition and configuration of the molecules. In a rough manner, we choose the adsorption rate constant to be proportional to the diffusion constant of the molecules, which in turn is determined by their size according to the Stokes–Einstein equation, Eq. (1). The molar volume, used to estimate the spherical molecule radius, is supposed to be proportional to the number of carbon atoms n. The reaction rate constant is chosen to be proportional to the area of the photocatalyst surface covered by the molecule. The remaining constants κ, and ϕ in Eqs. (21)–(23) are chosen to match the rate constants for the largest initial molecule.

To our knowledge, little is known about the dependence of the desorption rate constant on the size of the molecule in the case of aqueous solutions. For the desorption of organic molecules in vacuum, temperature-programmed desorption (TPD) studies [36] and molecular dynamics simulations [37] have been performed. For example, for the desorption of alkanes C_nH_{2n+2} from the MgO(100) surface, experimental investigations in [36] showed the desorption energy to depend linearly on the chain length n: $E_{\mathrm{des}}(n) = (6.5 + 7.1n)$ kJ mol^{-1}. The pre-exponential factor ν_0 strongly increased from $10^{13.1}$ to $10^{19.1}$ for n varying from 1 to 10. To what extent similar tendencies apply to desorption in aqueous solutions is not known. We consider, as a possible assumption in our model, that an analogous behavior occurs, where the desorption energy and pre-exponential factor depend on the molecule size in the following way

$$E_{\mathrm{des}}(n) = E_0 + E_1 n \tag{24}$$

$$\nu_0(n) = \alpha_0 10^{\alpha_1 n} \tag{25}$$

The parameters in these equations were chosen in a way that the desorption rate agrees with the rate derived from the initial organic molecules. As a consequence of such a *strong size dependence*, small intermediate molecules exhibit high desorption rates, leading to a small mineralization rate of these components. As demonstrated below, this results in a very slow decay of the TOC signal even after long exposure time. Such residual long-term TOC signals have been reported in [31,38–40].

The desorption rate of intermediates depends of course not only on the molecule size, but crucially also on their chemical structure. The TOC signal in many degradation studies has been observed to vanish completely after moderate illumination exposure [41]. For this reason, we consider also the case of *weak size dependence* of the desorption rate of intermediates. As a possible model function for this size dependence, we have chosen the simple relationship

$$k_{n,\mathrm{des}} = \beta_0 + \beta_1/n \tag{26}$$

with only two parameters. Because of its simplicity, relationship (26) facilitates parameter fits.

2.2.2.2. Fragmentation model. In this model, we consider the limiting case that photocatalytic reactions lead to the consecutive destruction of bonds in the molecules on the catalyst surface (Fig. 2b). Only the smallest fragments are mineralized. We study chain molecules, where the number of possible fragmentations of a molecule of size n is equal to $n-1$. The corresponding reaction equations for the species A_n are

$$\begin{aligned} A_n(\mathrm{aq}) \leftrightarrows A_n(\mathrm{ad}) &\rightarrow A_{(n-1)}(\mathrm{ad}) + M(\mathrm{aq}) \\ &\rightarrow A_{(n-2)}(\mathrm{ad}) + A_2(\mathrm{ad}) \\ &\rightarrow A_{(n-3)}(\mathrm{ad}) + A_3(\mathrm{ad}) \\ &\cdots \\ &\rightarrow M(\mathrm{aq}) + A_{(n-1)}(\mathrm{ad}) \end{aligned} \tag{27}$$

The concentration evolution for $n \geqslant 2$ is described by equations that are similar to the ones above

$$\frac{\mathrm{d}}{\mathrm{d}t}C_{A_n(\mathrm{ad})} = j_{n,\mathrm{ads}} - j_{n,\mathrm{des}} - j_{n,\mathrm{reac}} + j^*_{n,\mathrm{reac}} \tag{28}$$

$$\frac{\mathrm{d}}{\mathrm{d}t}C_{A_n(\mathrm{aq})} = a_s(j_{n,\mathrm{des}} - j_{n,\mathrm{ads}}) \tag{29}$$

$$\frac{\mathrm{d}}{\mathrm{d}t}C_{M(\mathrm{aq})} = a_s j^*_{1,\mathrm{reac}} \tag{30}$$

However, according to Eq. (27), several reaction pathways are possible for an adsorbed molecule. Thus, the evolution of an intermediate molecule of size n is influenced by the reactions of all larger molecules. This is included in the reaction flux as the sum over all possible fragmentations of larger molecules

$$j^*_{n,\mathrm{reac}} = \sum_{m=n+1}^{n_{\max}} \frac{2}{m-1} k_{m,\mathrm{reac}} C_{A_m(\mathrm{ad})} \tag{31}$$

Thereby, we have assumed that $m-1$ possible fragmentations of a molecule of size m occur with equal probability, leading to the weight factor $2/(m-1)$.

2.3. Numerical procedure

The evolution of the concentrations $C_{A_n(\mathrm{aq})}$, $C_{A_n(\mathrm{ad})}$, and $C_{M(\mathrm{aq})}$ was calculated in a python environment extended by the scipy modules [42]. The above system of differential equations was solved by means of the LSODA routine from the ODEPACK library [43] with a special python interface. The LSODA routine is a derivate of the Livermore Solver for Ordinary Differential Equations with the capability to switch automatically between a non-stiff and stiff solver depending on the behavior of the problem. The stiff solver uses backward differentiation formulas and the non-stiff solver an Adams predictor-corrector method.

3. Results and discussion

We present our calculated concentration evolutions of organic components in the aqueous solution based on the modeling approach proposed above. The specific surface area of nanoparticles, used in the calculations, was derived from BET measurements. For the P25 TiO_2 nanopowder, a value of 56 m^2 g^{-1} in agreement with reported data [44] was obtained, and for the ZnO nanopowder a value of 5.23 m^2 g^{-1}. The absorption rate constants k_{ads} were first determined from concentration measurements performed in the dark. The corresponding values, calculated by using Eq. (9), are listed in Table 1. These values have the same order of magnitude as reported in [45]. From the asymptotic concentration values measured at adsorption–desorption equilibrium, $C_{A(\mathrm{aq}),\infty}$, the desorption rate constants were determined by the use of Eqs. (10) and (11) (cf. Table 1). The data show that the adsorption rate of methylene blue on ZnO is smaller than that of ciprofloxacin. Comparing the two catalysts, one finds that adsorption on ZnO is about 20 times faster than on TiO_2. This demonstrates that ZnO

Table 1
Adsorption and desorption rate constants derived from experiments in the dark for the compounds ciprofloxacin (CIP) and methylene blue (MB) using photocatalysts TiO_2 and ZnO, respectively.

System	k_{ads} (m s^{-1})	k_{des} (s^{-1})
TiO_2–CIP	3.7×10^{-8}	2.05×10^{-2}
TiO_2–MB[a]	2.1×10^{-8}	2.85×10^{-2}
ZnO–CIP	7.5×10^{-7}	9.4×10^{-3}
ZnO–MB	5.4×10^{-7}	9.3×10^{-3}

[a] Fit from degradation experiment.

presents a more attractive surface for the tested organic molecules compared to TiO_2.

The results of our degradation experiments under UVA irradiation are shown in Fig. 3. To fit the measured data points within the framework of the single organic species model considered above, we used the adsorption rate constants derived from the adsorption experiments conducted in the dark. The fitting procedure revealed that all values for the reaction rate constant above a certain threshold fit the measured data points. From this observation, we conclude that adsorption of organic compounds was rate determining and that the reaction rate constant is greater than the desorption rate constant (cf. the discussion at the end of Section 2.2.1). To determine the adsorption rate constant for the system TiO_2–methylene blue k_{ads} was fitted to the degradation curve, assuming adsorption to be rate-determining.

Further experiments (Fig. 4a) with one half of the TiO_2 particle concentration revealed that the degradation of ciprofloxacin slows down with degradation half-life time differing by a factor of 2.05, i.e. close to the expected value 2. This corresponds to the model prediction in Eq. (13) where the rate constant is proportional to the specific particle surface a_s. Measurements of the ciprofloxacin concentration for degradation on TiO_2 with reduced UVA irradiation are shown in Fig. 4b. Remarkably, the curve fit yields a reaction rate constant $k_{reac} = 0.01\ s^{-1}$ which is one half of the desorption rate constant. According to the expression for the apparent rate constant Eq. (13), this means that at this irradiation intensity and below the degradation rate becomes reaction-limited.

The slight disagreement between the fitted exponential curve in Fig. 4b and the measurement data reflect presumably the limits of the single organic species model. Development and adsorption of intermediates could modify the degradation of ciprofloxacin.

Often, the concentration evolution of the initial organic compound can be well described by an exponential decay $\exp(-k_{app}t)$ with k_{app} as the apparent degradation rate constant [31,39,40,45] (cf. Eq. (12)). Also, measurements of the evolution of the total organic carbon (TOC) in the solution often show an exponential-like decay. There are, however, also studies where the TOC does not exhibit such behavior [31,38–40]. This is likely related to the mineralization kinetics of intermediate organic compounds. To demonstrate such complex degradation kinetics of the intermediates, Fig. 5 shows our calculated concentration evolutions of all intermediates.

In Fig. 5a, the case of a weak dependence of the desorption rates of intermediates on the molecule size n is considered (cf. Eq. (26)). For the incremental oxidation model (Fig. 5a) as well as for the fragmentation model (Fig. 5c), all intermediates are mineralized within moderate irradiation time. Clearly, the smallest intermediate needs the longest time since its desorption rate is the largest. For the incremental oxidation model, small intermediates emerge with some delay, whereas in the fragmentation model all compounds are produced with similar initial rates. In addition, for the latter model, particularly high concentrations of small intermediates arise, which are formed by fragmentation of all larger intermediates; this is contrary to the incremental oxidation mechanism.

The concentration curves in Fig. 5b and d demonstrate that a strong increase of the desorption rate of intermediates with decreasing molecule size (cf. Eq. (25)) strongly inhibits the complete mineralization of organic compounds in the solution. The smaller intermediates remain intact during long irradiation time. This is due to their high desorption rate, leading to a very low surface coverage. Possibly, these small intermediates could be oxidized to a noticeable extent by radicals in the aqueous solution. This reaction path was however neglected in the present model.

The characteristic concentration evolutions in Fig. 5 can be compared with experimental measurements. For example, the plots in Fig. 5c are similar to the evolution of certain intermediates during photocatalytic degradation of sulfamethoxazole observed in

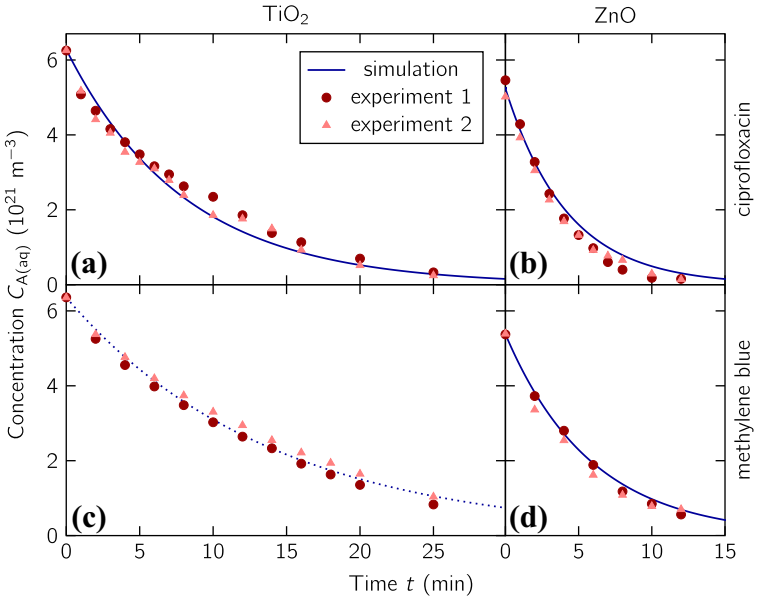

Fig. 3. Measured concentration evolutions during degradation of ciprofloxacin (a+b) and methylene blue (c+d) under UVA-irradiation with 1.0 g L^{-1} catalysts TiO_2 (a+c) and ZnO (b+d). The full lines represent fits according to the above single organic species model using the values of k_{ads} and k_{des} determined from experiments in the dark (Table 1). The dotted line in panel (c) was obtained by fitting k_{ads} from the degradation curve, assuming adsorption to be rate-determining.

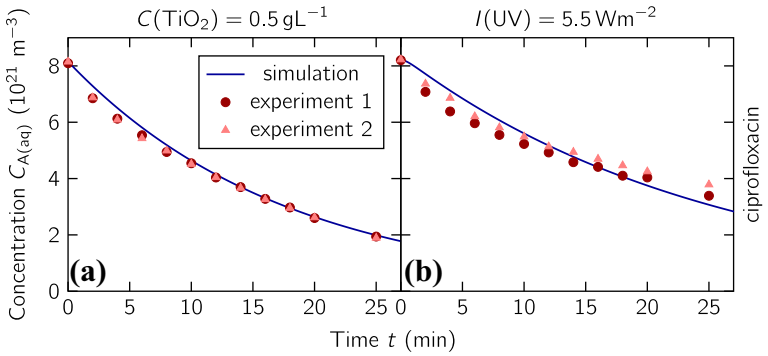

Fig. 4. Measured concentration evolutions during degradation of ciprofloxacin with TiO_2. Compared to Fig. 3a, a reduced TiO_2 particle concentration of 0.5 g L^{-1} (a), and a lower UVA-irradiation of 5.5 W m^{-2} (b) was used. The lines represent fits according to the single organic species model using the values of k_{ads} and k_{des} determined from the dark experiments (Table 1). The fitted reaction constant in panel (b) is $k_{reac} = 0.01\,s^{-1}$.

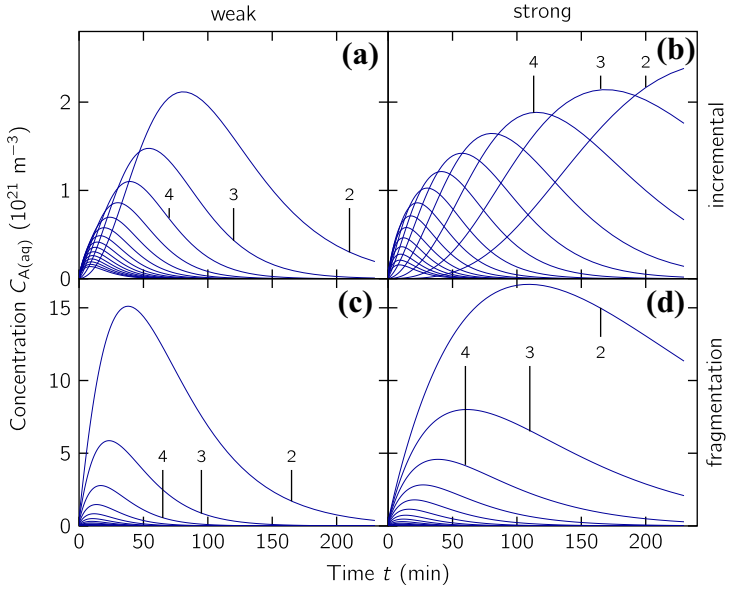

Fig. 5. Calculated concentration evolutions of intermediates of size n (curve label) based on the incremental oxidation (a+b) or fragmentation (c+d) model with weak (a+c) or strong (b+d) dependence of the desorption rate constants on the molecule size n according to Eqs. (24)–(26). Parameters: $n_{max} = 17$, $a_s = 56,000\ m^{-1}$, $\kappa = 61.5$, $I_0\phi = 3.81 \times 10^{17}\ s^{-1}m^{-2}$; weak: $\beta_1 = 0.8\ s^{-1}$, $\beta_0 = -0.029\ s^{-1}$; strong: $E_1 = 3.0$ kJ mol^{-1}, $E_0 = 44.0$ kJ mol^{-1}, $\alpha_1 = 0.412$, $\alpha_0 = 1.51 \times 10^8\ s^{-1}$.

[14]. Also in the case of the intensively studied degradation of phenol [27,26], the intermediate concentrations show a similar form to Fig. 5c. The evolution of reaction intermediates has been explored also for the gas phase oxidation of decane [46]. Many intermediates show concentration evolutions similar to Fig. 5c. However, there are also few crossings of concentration profiles as seen in Fig. 5b.

The total amount of organic compounds remaining in the solution after irradiation is commonly characterized by measuring the TOC. For this reason, we have also calculated the evolution of the TOC within our proposed models. Fig. 6 displays the characteristic differences of the TOC evolution between the two degradation mechanisms discussed above. For weak size dependence of the desorption rate of intermediates, the incremental oxidation mechanism under moderate irradiation shows an exponential-like decay of the TOC signal as the organic material disappears. For the fragmentation mechanism and weak size dependence of the desorption rates of intermediates, the TOC curve shows an inflection point at the beginning (at about 10–20 min). This slight initial delay in the TOC signal reduction is caused by the fact that only the smallest fragments are mineralized. Their formation obviously needs a certain amount of time. In the case of the incremental

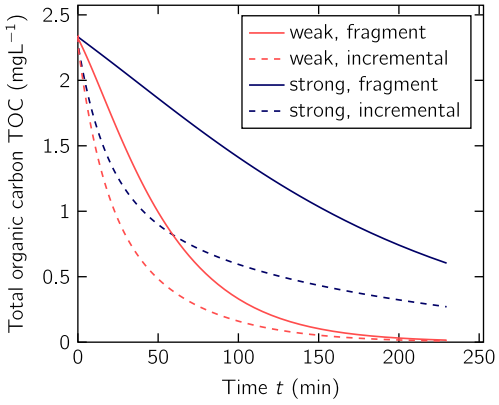

Fig. 6. Comparison between the TOC evolution for the incremental oxidation and the fragmentation model for weak and strong size dependence of the desorption rate. Parameters as in Fig. 5.

degradation mechanism and strong size dependence of the desorption rate, the TOC signal shows a fast initial decrease followed by a considerably slower decay, whereas the fragmentation mechanism

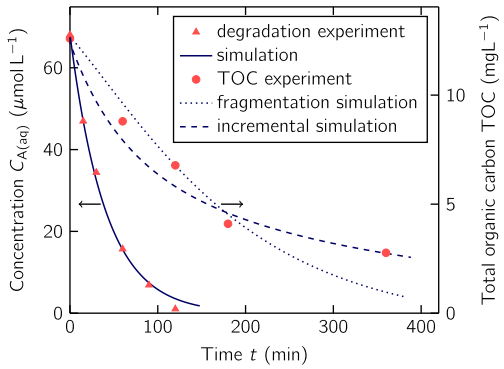

Fig. 7. Simulation results for the degradation of methylene blue by TiO_2 based on data reported in [31] ($a_s = 140,000\ m^{-1}$). The full line is a fit according to the single organic species model. The resulting parameters ($k_{ads} = 3.0 \times 10^{-9}\ ms^{-1}$, $k_{des} = 6.8 \times 10^{-3}\ s^{-1}$) were used for fitting the TOC curves. For the reaction constant $k_{reac} = 10k_{des}$ was chosen. The desorption behavior of the intermediates was modeled by Eq. (26) with $n_{max} = 16$ (fragmentation model: $\beta_0 = -6.57 \times 10^{-3}\ s^{-1}$, $\beta_1 = 0.122\ s^{-1}$; incremental oxidation model: $\beta_0 = -3.06 \times 10^{-2}\ s^{-1}$, $\beta_1 = 0.496\ s^{-1}$).

shows a slower initial decrease. For both degradation mechanisms with strong size dependence of the desorption rate, a certain amount of the organic compounds remains after reasonable irradiation exposure.

The degradation of methylene blue on TiO_2 and the corresponding TOC evolution was studied by Houas et al. [31]. From the presented adsorption experiments, we extracted the adsorption and desorption rate constants, given in Fig. 7. Differences to the values found in our experiments can be due to different pH values of the solutions. Analysis of the degradation data within the single organic species model suggested that the degradation is adsorption-limited, i.e. k_{reac} is considerably larger than k_{des}. Thus, we have chosen $k_{reac} = 10k_{reac}$ in our simulations. Fig. 7 shows our simulation results for the TOC data in [31] obtained within our incremental oxidation and fragmentation models and using Eq. (26) for the description of the desorption behavior of intermediates. The number of intermediates was roughly chosen as the number of carbon atoms in methylene blue ($n_{max} = 16$). Comparison of the fitted TOC curves in Fig. 7 with the experimental data shows that both models give no complete agreement. The long-term evolution seems better fitted by the incremental oxidation model, presumably after initially dominant fragmentation has occurred. Clearly, for a detailed quantitative understanding of TOC measurements as well as of the evolution of intermediates, the knowledge of their species-specific adsorption–desorption properties is of great importance.

4. Conclusions

An extended modeling approach for the simulation of the degradation of organic molecules in water by means of photocatalytic nanosuspensions was presented. The model includes the formation of intermediate organic components either by incremental oxidation or by fragmentation of molecules. Rate constants in the model were determined by comparison with experimental findings on four model systems (ciprofloxacin or methylene blue combined with photocatalysts TiO_2 or ZnO). The adsorption rates for ZnO were considerably higher compared to TiO_2. Fitting our simulations to the measurements showed that adsorption of the organic molecules on the photocatalyst was the rate determining process for sufficiently high UVA-irradiation of about $20\ W\ m^{-2}$. By decreasing the intensity, the photocatalytic reaction on the catalyst surface becomes rate determining. Our simulations of the TOC evolution reveal that high desorption rates of small intermediate molecules cause a slow long-term decay of the TOC signal.

For a more realistic simulation of the degradation process, the idealized incremental oxidation and fragmentation mechanisms of the present model can be modified by species-specific reaction paths. Our modeling approach should also be applicable for the simulation of air purification. In particular, for air purification systems, adsorption and desorption rate constants for many molecules have been reported in the literature [46] .

Acknowledgements

This work is funded by the European Union (ERDF) and the Free State of Saxony via the ESF project 100098212 InnoMedTec. We thank Henrik Frenzel, Virginia Gómez Jiménez, and Li Li for support with the experimental work, as well as Markus Pötschke, Quirina Roode-Gutzmer, Pedro Martins, and Hoai Nga Le for their many useful discussions.

Appendix A. Analytical solution

For the single organic species model, the solution of Eqs. (3) and (4) in the limiting case $\Theta \ll 1$ is given by

$$C_{A(aq)}(t) = k_1 \exp(\lambda_1 t) + k_2 \exp(\lambda_2 t) \tag{A.1}$$

$$C_{A(ad)}(t) = k_1 \frac{\lambda_1 + a_s k_{ads}}{a_s k_{des}} \exp(\lambda_1 t) + k_2 \frac{\lambda_2 + a_s k_{ads}}{a_s k_{des}} \exp(\lambda_2 t) \tag{A.2}$$

$$k_1 = \frac{a_s k_{des} C_{A(ad),0} - (a_s k_{ads} + \lambda_2) C_{A(aq),0}}{\lambda_1 - \lambda_2} \tag{A.3}$$

$$k_2 = \frac{a_s k_{des} C_{A(ad),0} - (a_s k_{ads} + \lambda_1) C_{A(aq),0}}{\lambda_2 - \lambda_1} \tag{A.4}$$

$$\lambda_1 = -\frac{1}{2}\left(\vartheta_0 + \left(\vartheta_0^2 - 4a_s k_{ads} k_{reac}\right)^{1/2}\right) \tag{A.5}$$

$$\lambda_2 = -\frac{1}{2}\left(\vartheta_0 - \left(\vartheta_0^2 - 4a_s k_{ads} k_{reac}\right)^{1/2}\right) \tag{A.6}$$

$$\vartheta_0 = a_s k_{ads} + k_{des} + k_{reac} \tag{A.7}$$

References

[1] C.G. Daughton, B.W. Brooks, Active pharmaceutical ingredients and aquatic organisms, in: B.W. Nelson (Ed.), Environ. Contam. Biota Interpret. Tissue Conc., CRC Press, 2011, pp. 255–280.
[2] B. Halling-Sørensen, S. Nors Nielsen, P. Lanzky, F. Ingerslev, H. Holten Lützhøft, S. Jørgensen, Occurrence, fate and effects of pharmaceutical substances in the environment – a review, Chemosphere 36 (1998) 357–393.
[3] M.D. Hernando, M. Mezcua, A.R. Fernández-Alba, D. Barceló, Environmental risk assessment of pharmaceutical residues in wastewater effluents, surface waters and sediments, Talanta 69 (2006) 334–342.
[4] I. Michael, L. Rizzo, C.S. McArdell, C.M. Manaia, C. Merlin, T. Schwartz, C. Dagot, D. Fatta-Kassinos, Urban wastewater treatment plants as hotspots for the release of antibiotics in the environment: a review, Water Res. 47 (2013) 957–995.
[5] K.T. Chung, G.E. Fulk, A.W. Andrews, Mutagenicity testing of some commonly used dyes, Appl. Environ. Microbiol. 42 (1981) 641–648.
[6] R.O. Alves de Lima, A.P. Bazo, D.M.F. Salvadori, C.M. Rech, D. de Palma Oliveira, G. de Aragão Umbuzeiro, Mutagenic and carcinogenic potential of a textile azo dye processing plant effluent that impacts a drinking water source, Mutat. Res. 626 (2007) 53–60.
[7] D.S. Bhatkhande, V.G. Pangarkar, A.A. Beenackers, Photocatalytic degradation for environmental applications – a review, J. Chem. Technol. Biotechnol. 77 (2002) 102–116.
[8] S. Malato, P. Fernández-Ibáñez, M. Maldonado, J. Blanco, W. Gernjak, Decontamination and disinfection of water by solar photocatalysis: recent overview and trends, Catal. Today 147 (2009) 1–59.

[9] K. Kabra, R. Chaudhary, R.L. Sawhney, Treatment of hazardous organic and inorganic compounds through aqueous-phase photocatalysis: a review, Ind. Eng. Chem. Res. 43 (2004) 7683–7696.
[10] M.N. Chong, B. Jin, C.W.K. Chow, C. Saint, Recent developments in photocatalytic water treatment technology: a review, Water Res. 44 (2010) 2997–3027.
[11] F. Haque, E. Vaisman, C.H. Langford, A. Kantzas, Preparation and performance of integrated photocatalyst adsorbent (IPCA) employed to degrade model organic compounds in synthetic wastewater, J. Photochem. Photobiol. A Chem. 169 (2005) 21–27.
[12] I.K. Konstantinou, T. Albanis, TiO_2-assisted photocatalytic degradation of azo dyes in aqueous solution: kinetic and mechanistic investigations, Appl. Catal. B Environ. 49 (2004) 1–14.
[13] M. Faramarzpour, M. Vossoughi, M. Borghei, Photocatalytic degradation of furfural by titania nanoparticles in a floating-bed photoreactor, Chem. Eng. J. 146 (2009) 79–85.
[14] L. Hu, P.M. Flanders, P.L. Miller, T.J. Strathmann, Oxidation of sulfamethoxazole and related antimicrobial agents by TiO_2 photocatalysis, Water Res. 41 (2007) 2612–2626.
[15] F. Thevenet, O. Guaïtella, J. Herrmann, A. Rousseau, C. Guillard, Photocatalytic degradation of acetylene over various titanium dioxide-based photocatalysts, Appl. Catal. B Environ. 61 (2005) 58–68.
[16] K. Hashimoto, H. Irie, A. Fujishima, TiO_2 photocatalysis: a historical overview and future prospects, Jpn. J. Appl. Phys. 44 (2005) 8269–8285.
[17] A. Fujishima, T.N. Rao, D.A. Tryk, Titanium dioxide photocatalysis, J. Photochem. Photobiol. C Photochem. Rev. 1 (2000) 1–21.
[18] A.E. Cassano, C.A. Martin, R.J. Brandi, O.M. Alfano, Photoreactor analysis and design: fundamentals and applications, Ind. Eng. Chem. Res. 34 (1995) 2155–2201.
[19] M. Motegh, J. Cen, P.W. Appel, J.R. van Ommen, M.T. Kreutzer, Photocatalytic-reactor efficiencies and simplified expressions to assess their relevance in kinetic experiments, Chem. Eng. J. 207–208 (2012) 607–615.
[20] V. Vaiano, O. Sacco, M. Stoller, A. Chianese, P. Ciambelli, D. Sannino, Influence of the photoreactor configuration and of different light sources in the photocatalytic treatment of highly polluted wastewater, Int. J. Chem. React. Eng. 12 (2014) 1–13.
[21] C. Minero, Kinetic analysis of photoinduced reactions at the water semiconductor interface, Catal. Today 54 (1999) 205–216.
[22] R. Andreozzi, V. Caprio, A. Insola, G. Longo, V. Tufano, Photocatalytic oxidation of 4-nitrophenol in aqueous TiO_2 slurries: an experimental validation of literature kinetic models, J. Chem. Technol. Biotechnol. 75 (2000) 131–136.
[23] D. Sannino, V. Vaiano, O. Sacco, P. Ciambelli, Mathematical modelling of photocatalytic degradation of methylene blue under visible light irradiation, J. Environ. Chem. Eng. 1 (2013) 56–60.
[24] C.-H. Wu, J.-M. Chern, Kinetics of photocatalytic decomposition of methylene blue, Ind. Eng. Chem. Res. 45 (2006) 6450–6457.
[25] G. Li Puma, B. Toepfer, A. Gora, Photocatalytic oxidation of multicomponent systems of herbicides: scale-up of laboratory kinetics rate data to plant scale, Catal. Today 124 (2007) 124–132.
[26] J. Moreira, B. Serrano, A. Ortiz, H. de Lasa, A unified kinetic model for phenol photocatalytic degradation over TiO_2 photocatalysts, Chem. Eng. Sci. 78 (2012) 186–203.
[27] M. Salaices, B. Serrano, H. de Lasa, Photocatalytic conversion of phenolic compounds in slurry reactors, Chem. Eng. Sci. 59 (2004) 3–15.
[28] M. El-Kemary, H. El-Shamy, I. El-Mehasseb, Photocatalytic degradation of ciprofloxacin drug in water using ZnO nanoparticles, J. Lumin. 130 (2010) 2327–2331.
[29] T.G. Vasconcelos, D.M. Henriques, A. König, A.F. Martins, K. Kümmerer, Photo-degradation of the antimicrobial ciprofloxacin at high pH: identification and biodegradability assessment of the primary by-products, Chemosphere 76 (2009) 487–493.
[30] T. Paul, M.C. Dodd, T.J. Strathmann, Photolytic and photocatalytic decomposition of aqueous ciprofloxacin: transformation products and residual antibacterial activity, Water Res. 44 (2010) 3121–3132.
[31] A. Houas, Photocatalytic degradation pathway of methylene blue in water, Appl. Catal. B Environ. 31 (2001) 145–157.
[32] C.R. Wilke, P. Chang, Correlation of diffusion coefficients in dilute solutions, AIChE J. 1 (1955) 264–270.
[33] J. Crank, The Mathematics of Diffusion, Clarendon Press, Oxford, 1975.
[34] M. Connolly, Solvent-accessible surfaces of proteins and nucleic acids, Science 221 (1983) 709–713.
[35] L. Schrödinger, The PyMOL Molecular Graphics System, Version 1.3r1, 2013. <http://pymol.org>.
[36] S.L. Tait, Z. Dohnálek, C.T. Campbell, B.D. Kay, n-Alkanes on MgO(100). II. Chain length dependence of kinetic desorption parameters for small n-alkanes, J. Chem. Phys. 122 (2005) 164708.
[37] K.A. Fichthorn, K.E. Becker, R.A. Miron, Molecular simulation of temperature-programmed desorption, Catal. Today 123 (2007) 71–76.
[38] F.J. Beltrán, A. Aguinaco, J.F. García-Araya, Mechanism and kinetics of sulfamethoxazole photocatalytic ozonation in water, Water Res. 43 (2009) 1359–1369.
[39] M.M. Mohamed, M.M. Al-Esaimi, Characterization, adsorption and photocatalytic activity of vanadium-doped TiO_2 and sulfated TiO_2 (rutile) catalysts: degradation of methylene blue dye, J. Mol. Catal. A Chem. 255 (2006) 53–61.
[40] T. Zhang, T.K. Oyama, S. Horikoshi, H. Hidaka, J. Zhao, N. Serpone, Photocatalyzed N-demethylation and degradation of methylene blue in titania dispersions exposed to concentrated sunlight, Sol. Energy Mater. Sol. Cells 73 (2002) 287–303.
[41] C. Minero, G. Mariella, V. Maurino, E. Pelizzetti, Photocatalytic transformation of organic compounds in the presence of inorganic anions. 1. Hydroxyl-mediated and direct electron-transfer reactions of phenol on a titanium dioxidefluoride system, Langmuir 16 (2000) 2632–2641.
[42] T.E. Oliphant, Python for scientific computing, Comput. Sci. Eng. 9 (2007) 10–20.
[43] A.C. Hindmarsh, ODEPACK, a systematized collection of ODE solvers, in: R.S. Stepleman (Ed.), Sci. Comput., Amsterdam, 1983, pp. 55–64.
[44] K.J.A. Raj, B. Viswanathan, Effect of surface area, pore volume and particle size of P25 titania on the phase transformation of anatase to rutile, Indian J. Chem. 48A (2009) 1378–1382.
[45] H. Chang, C. Su, C. Lo, L. Chen, T. Tsung, C. Jwo, Photodecomposition and surface adsorption of methylene blue on TiO_2 nanofluid prepared by ASNSS, Mater. Trans. 45 (2004) 3334–3337.
[46] O. Debono, F. Thévenet, P. Gravejat, V. Héquet, C. Raillard, L. Le Coq, N. Locoge, Gas phase photocatalytic oxidation of decane at ppb levels: removal kinetics, reaction intermediates and carbon mass balance, J. Photochem. Photobiol. A Chem. 258 (2013) 17–29.